

ONLINE LEARNING OF BOTH STATE AND DYNAMICS USING ENSEMBLE KALMAN FILTERS

MARC BOCQUET*, ALBAN FARCHI AND QUENTIN MALARTIC

CEREA, joint laboratory École des Ponts ParisTech and EDF R&D,
Université Paris-Est, Champs-sur-Marne, France

(Communicated by the associate editor name)

ABSTRACT. The reconstruction of the dynamics of an observed physical system as a surrogate model has been brought to the fore by recent advances in machine learning. To deal with partial and noisy observations in that endeavor, machine learning representations of the surrogate model can be used within a Bayesian data assimilation framework. However, these approaches require to consider long time series of observational data, meant to be assimilated all together. This paper investigates the possibility to learn both the dynamics and the state online, i.e. to update their estimates at any time, in particular when new observations are acquired. The estimation is based on the ensemble Kalman filter (EnKF) family of algorithms using a rather simple representation for the surrogate model and state augmentation. We consider the implication of learning dynamics online through (i) a global EnKF, (ii) a local EnKF and (iii) an iterative EnKF and we discuss in each case issues and algorithmic solutions. We then demonstrate numerically the efficiency and assess the accuracy of these methods using one-dimensional, one-scale and two-scale chaotic Lorenz models.

1. Introduction.

1.1. Learning the dynamics of a model: a time-dependent variational problem. There has been a surge of studies that aim at reconstructing the dynamics of a physical system from its sole observation. The key output of these studies is a surrogate model meant to emulate the dynamical system. This trend has been triggered by the significant advances in machine learning (ML), and in particular neural networks (NNs), over the past decade. Chaotic systems are of particular interest because of their prevalence in geophysical flows, but also because of their intrinsic instability and poor predictability making this endeavor a difficult one. Several ML techniques have been tested when focusing on the reconstruction of chaotic dynamics: the analogs [37], the projection of the dynamics resolvent onto nonlinear regressors (e.g., [42, 16]), echo state networks (e.g., [43]), and residual NNs to represent either the resolvent (e.g., [20, 51, 15]) or underlying ordinary differential equations (ODEs) (e.g., [22, 38, 8, 9]). The ML techniques developed in these references are evaluated on chaotic low-order models such as the Lorenz-96

2010 *Mathematics Subject Classification.* Primary: 62M20, 65C60; Secondary: 86-08.

Key words and phrases. data assimilation, machine learning, chaotic dynamical systems, parameter estimation, ensemble Kalman filter, local ensemble Kalman filter, iterative ensemble Kalman filter.

* Corresponding author: Marc Bocquet.

model (L96, [40]) or the two-scale Lorenz model (L05III, [39]). Moreover, the NN and reservoir models in [20, 51, 52, 3] were tested on genuine meteorological fields.

In all these studies, the learning step is a variational problem which consists in optimizing a loss function. The latter crucially depends on the entire sequence of observations representing a long system trajectory, even though the observations can be exploited by batches, for instance when using stochastic optimization.

1.2. A Bayesian framework combining data assimilation and machine learning. In practice, most of these studies consider that the physical system is fully and noiselessly observed. Some very weak noise can nonetheless be added to the observations for regularization of the learning scheme [6]. However, a Bayesian formalism that extends ML approaches, including NN representations, to the case of partial and noisy observations, has recently been developed. Brajard et al. [15] have first shown how to combine ML with data assimilation (DA) to be able to process noisy and partial observations. In their scheme, DA is used as an advanced space-time interpolation tool, which alternates with a refined estimation of the surrogate model through the optimization of the NN coefficients. This has been framed into a unifying Bayesian formalism in [9], which allows to develop approximations and alternative algorithms. The typical tool of the DA step is the ensemble Kalman smoother (EnKS), while the ML step relies on ML libraries such as TensorFlow or Pytorch. Although this approach is theoretically scalable to high-dimensional systems, it is obviously more complex than the isolated ML step. As emphasized in Section 1.1, the approach is offline as it requires the full observation dataset for the ML step.

Given a set of observations $\mathbf{y}_{0:K} = \{\mathbf{y}_k\}_{0 \leq k \leq K} \in \mathbb{R}^{(K+1) \times N_y}$, a typical ML loss function is

$$\mathcal{J}(\mathbf{p}) = \frac{1}{2} \sum_{k=1}^K \|\mathbf{y}_k - \mathbf{F}^{k-1}(\mathbf{p}, \mathbf{y}_{k-1})\|^2 + \mathcal{L}(\mathbf{p}), \quad (1)$$

where $\mathbf{x} \mapsto \mathbf{F}^{k-1}(\mathbf{p}, \mathbf{x})$ is the resolvent of the surrogate model integrated from t_{k-1} to t_k , \mathbf{p} is the set of coefficients used in the mathematical representation of the surrogate model (for instance the weights and biases of a NN), and $\mathcal{L}(\mathbf{p})$ is the regularization term of the surrogate model, which, from a Bayesian standpoint, corresponds to a prior on the surrogate model.

In (1), the surrogate model is supposed to be autonomous, such that \mathbf{p} does not depend on time. Generalizations are possible though, such as a slow evolution of the dynamics, or when considering a dynamical autonomous core parameterized by \mathbf{p} together with time-dependent parameters representing time-dependent forcings. However, these generalizations will not be addressed in this paper, so that the surrogate model will be assumed autonomous throughout the paper.

Equation (1) is a limiting case of the more general cost function [31, 1, 8, 9]:

$$\begin{aligned} \mathcal{J}(\mathbf{p}, \mathbf{x}_{0:K}) &= \frac{1}{2} \sum_{k=0}^K \|\mathbf{y}_k - \mathbf{H}_k(\mathbf{x}_k)\|_{\mathbf{R}_k}^2 \\ &\quad + \frac{1}{2} \sum_{k=1}^K \|\mathbf{x}_k - \mathbf{F}^{k-1}(\mathbf{p}, \mathbf{x}_{k-1})\|_{\mathbf{Q}_k}^2 + \mathcal{L}(\mathbf{p}, \mathbf{x}_0), \end{aligned} \quad (2)$$

where $\mathbf{x}_{0:K} = \{\mathbf{x}_k\}_{0 \leq k \leq K} \in \mathbb{R}^{(K+1) \times N_x}$ is the unknown state trajectory, $\{\mathbf{H}_k\}_{0 \leq k \leq K}$ are the observation operators from \mathbb{R}^{N_x} to \mathbb{R}^{N_y} . If need be, the observation space

dimension N_y can be made time-dependent. The norm notation $\|\mathbf{x}\|_{\mathbf{G}}$ stands for the Mahalanobis distance $\sqrt{\mathbf{x}^\top \mathbf{G} \mathbf{x}}$. This cost function is derived from Bayes' rule assuming Gaussian statistics for the errors: the observation errors have no bias and covariance matrices $\{\mathbf{R}_k\}_{0 \leq k \leq K}$ and the model errors have no bias and covariance matrices $\{\mathbf{Q}_k\}_{0 \leq k \leq K}$. It is also assumed that these errors are uncorrelated in time and that model and observation errors are uncorrelated. $\mathcal{L}(\mathbf{p}, \mathbf{x}_0)$ is the regularization term for the surrogate model coefficients \mathbf{p} and for the initial state \mathbf{x}_0 of the trajectory, and can be derived from the prior distribution on \mathbf{p} and \mathbf{x}_0 . The observation and model error statistics, i.e. \mathbf{R}_k and \mathbf{Q}_k , are not considered part of the control variables, i.e. of the variable to be estimated. This latter topic has been investigated in [9] and will not be dealt with in the present paper, as it would add another significant layer of complexity.

1.3. Investigating theoretical aspects of online schemes. Our goal in this study is to investigate the possibility to learn both the state and the dynamics online, i.e. assimilate the new batches of observations, which are possibly sparse and noisy, when they arrive, and subsequently update the surrogate model and state estimates.

If the full observation dataset was available, the problem could be solved using the cost function (2). In practice with realistically noisy systems, one would have to use one of the algorithms described in [15, 9]. However, since we assume that the batches of observations are gradually acquired, this requires the development of a sequential algorithm instead. Our focus is on the theoretical and algorithmic aspects of the problem. Rasp [45] has investigated a similar problem but focused on possible solutions for numerical weather prediction centers, in particular relying on the use of an existing imperfect model for the physical system. Our approach has more to do with the extension of known DA methods to ML problems.

A simple algorithm one can think of is the augmented state ensemble Kalman filter (EnKF), where the state variable \mathbf{x} is extended to incorporate the coefficients of the model representation (\mathbf{x}, \mathbf{p}) following the principle introduced in [34]. The augmentation principle is elegant, simple and has already been used for parameterized model error or forcings in DA and inverse problems (see [47] for a review and references in the geosciences).

However, applying the augmented EnKF to the full model is numerically challenging. It also raises many issues when considering more advanced schemes such as local EnKFs [30, 28, 21] needed for high-dimensional estimation problems and iterative EnKFs [50, 13, 49] meant to better deal with model nonlinearities.

The goal of this paper is to investigate algorithmically (i) the simple augmented EnKF for model and state reconstruction, as well as its advanced variants based on (ii) local EnKFs and on (iii) iterative EnKFs. Moreover, we want to numerically assess these algorithms on low-order chaotic models.

1.4. Outline. In Section 2, we discuss choices to be made for the surrogate model mathematical representation, which may have an impact on the design of the augmented EnKF. In Section 3, we define the augmented-state EnKF based on a ML surrogate model, introduce and develop the associated local EnKF, as well as the corresponding iterative EnKF. These methods are evaluated on the L96 and L05III one-dimensional low-order chaotic models in Section 4. Conclusions are drawn in Section 5.

2. Surrogate model representation. Because the augmented EnKF is flexible, any adequate representation of the dynamics parameterized by a vector of coefficients \mathbf{p} can a priori be chosen as the surrogate model. The main constraint is that the physical dynamics should project significantly onto the set of surrogate models generated by these parameters. Another important constraint which is inherent to the choice of the EnKF and more fundamentally to the sequential approach, is that the number of coefficients N_p in \mathbf{p} must be limited. This may rule out deep NNs with a large number of weights and biases, but more compact residual NNs based on convolutional layers could certainly be chosen as the surrogate model. If such NN is implemented with TensorFlow or Pytorch, a bonus would be that the adjoint of the surrogate model could easily be obtained, since these tools come with automatic differentiation. This is superfluous for the global and local EnKF since the adjoint is not required. By contrast, even though the adjoint is not strictly required, it could nevertheless be useful in the iterative EnKF or its local variant [7], because the iterative EnKF piggybacks on a nonlinear variational analysis.

In the numerical applications of this study, we will choose the monomial representation described in Sections 2.1 and 2.2 of [8]. It is an ODE representation of the surrogate dynamics even though the physical model could either be governed by ODEs or partial differential equations (PDEs). The monomials are used to parameterize the flow rate, i.e. the equations of the surrogate model, which is later integrated in time using an appropriate numerical integration scheme (typically a fourth-order Runge–Kutta scheme) to build the resolvent $\mathbf{x}_k \mapsto \mathbf{F}^k(\mathbf{p}, \mathbf{x}_k)$ between two time steps. Note that this representation is equivalent to a NN, and can be either be implemented straightforwardly (as in [8]) or using TensorFlow or Pytorch (as in [9]). Explicit details can be found in [8, 9].

We make the assumption of locality of the dynamics, which reduces considerably the number of coefficients of the representation which then scales as the size of the system, see Section 2.2.1 of [8]. The mathematical description of the dynamics is local and only makes use of variables within a given stencil. We further assume homogeneity of the system, see Section 2.2.2 of [8], i.e. translational invariance of the dynamics. This assumption is less realistic but often satisfied by the dynamical part of the model, while forcing terms could realistically be spatially inhomogeneous. In the end, the number of coefficients N_p is considerably reduced by making these assumptions. Both assumptions will be enforced hereafter, but homogeneity will be questioned to some extent in the following.

3. Ensemble Kalman-based methods. As explained in the introduction, Section 1.3, the augmented EnKF consists in extending the state vector $\mathbf{x} \in \mathbb{R}^{N_x}$ to

$$\mathbf{z} = \begin{bmatrix} \mathbf{x} \\ \mathbf{p} \end{bmatrix} \in \mathbb{R}^{N_z}, \quad (3)$$

with $N_z = N_x + N_p$. The ensemble of the filter is made of such augmented vectors. Although the coefficients of $\mathbf{p} \in \mathbb{R}^{N_p}$ are not observed, correlations between the state vector and the model parameters will implicitly be formed in the ensemble through the analysis. The best state/model couple will thrive in the forecast step and be subsequently favored in the analysis step by getting a larger contribution.

If the principle is well-known [34, 47], seeking a surrogate for the whole model is a bolder endeavor. It also has important implications on the implementation of the local and of the iterative EnKFs, two fundamentally important variants of the

EnKF. In the rest of the paper, we will call EnKF-ML a variant of the EnKF with its state vector augmented with all surrogate model parameters.

3.1. The ensemble Kalman filter. At time t_k , the basic EnKF-ML has its analysis step built on the cost function

$$\mathcal{J}_k(\mathbf{z}_k) = \frac{1}{2} \|\mathbf{y}_k - \boldsymbol{\Theta}_k(\mathbf{z}_k)\|_{\mathbf{R}_k^{-1}}^2 + \frac{1}{2} \|\mathbf{z}_k - \mathbf{z}_k^f\|_{\mathbf{B}_k^{-1}}^2, \quad (4)$$

where $\mathbf{z}_k = [\mathbf{x}_k^\top \ \mathbf{p}_k^\top]^\top \in \mathbb{R}^{N_z}$ and $\boldsymbol{\Theta}_k = [\mathbf{H}_k \ \mathbf{0}]$ is the augmented observation operator. $\mathbf{B}_k \in \mathbb{R}^{N_z \times N_z}$ is the error covariance matrix of \mathbf{z}_k estimated with the sample statistics of the augmented state ensemble¹. The EnKF-ML has the same implementation as the EnKF albeit with the augmented state/model \mathbf{z}_k . In the numerical evaluation of Section 4, we choose for the EnKF-ML an implementation based on either the ensemble transform Kalman filter (ETKF, [4, 33]), or the ensemble square root Kalman filter (EnSRF, [53]).

For the state \mathbf{x}_k , the forecast step from t_k to t_{k+1} is based on the application of the resolvent $\mathbf{x} \mapsto \mathbf{F}^k(\mathbf{p}, \mathbf{x})$. The forecast of the parameter is chosen to be persistence since we assumed the dynamics to be autonomous (\mathbf{p}_k is in principle constant in time). Because the reconstructed dynamics is certainly flawed, with the academic exception of the perfect reconstruction of identifiable true dynamics, one has to account for model error in the forecast of the state, for instance using the simple deterministic SQRT-CORE algorithm of [44], and/or using multiplicative inflation.

Because the augmented dynamics acting on \mathbf{z}_k are based on persistence for the parameters, it is clear that their Lyapunov spectrum will be that of $\mathbf{x} \mapsto \mathbf{F}^k(\mathbf{p}_k, \mathbf{x})$ with the addition of N_p neutral modes, i.e. of exponent 0, due to the neutral dynamics of the model parameters². If the estimation of the physical model is accurate enough, the spectrum of $\mathbf{x} \mapsto \mathbf{F}^k(\mathbf{p}_k, \mathbf{x})$ should be close to that of the true dynamics. Assuming that N_0 is the dimension of the unstable and neutral subspace of the true dynamics, the dimension of the unstable and neutral subspace of the augmented dynamics should be about $N_0 + N_p$. As a consequence, following [10, 27], the size of the (centered) ensemble should at least satisfy

$$N_e \gtrsim N_0 + N_p + 1, \quad (5)$$

in order to avoid divergence without resorting to localization. From the theoretical and numerical results of [12] on the impact of the neutral modes on the collapse of the forecast error covariance matrix on the unstable and neutral subspace, we expect that the filter would diverge for $N_e \leq N_0$ and we expect that the accuracy of the filter would gradually improve in the range $N_0 + 1 \leq N_e \leq N_0 + N_p + 1$. The filter's accuracy can however still improve when $N_e > N_0 + N_p + 1$, as the need for inflation is increasingly reduced.

3.2. The local ensemble Kalman filter. In this section, we discuss of the implementation of a local EnKF-ML (LEnKF-ML). As explained above, whenever $N_e < N_0 + N_p + 1$ localization was surmised to be beneficial, if not necessary.

¹For the prior term in (4) to make sense, one can assume \mathbf{B}_k to be invertible either by regularization, typically localization, or because its inverse can always be defined in the ensemble subspace.

²This would also be true for additive stochastic perturbations applied to the parameters.

3.2.1. Localization and statistical homogeneity of the parameters. The strategy chosen to make the filter local primarily depends on the nature of the surrogate model parameters \mathbf{p} . If the observed dynamical system is heterogeneous, the surrogate model representation should be heterogeneous as well, and \mathbf{p} should depend on space location. Hence those parameters are local. In this case, the application of either local analysis/domain localization (DL) or covariance localization (CL) is in principle straightforward. For DL, the update is performed locally for both the state and parameters, i.e. on the joint vector \mathbf{z} . The updated ensemble can directly be formed from these local updates. In this case, only local domains and possibly a tapering function for the observation precision matrix have to be specified as in standard EnKF DL. For CL, the localization matrix, to be used in the Schur product, can be defined using the physical distance between two state variables, two parameters, or a state variable and a parameter. One could also think of a more complex localization matrix with two localization lengths, one for the state variables and one for the parameters. Yet, one should check that the resulting correlation matrix is positive semi-definite.

These local parameter approaches are very appealing for the tentative LEnKF-ML. However, they would lead to severe underdetermination, especially in the sequential context of this study. There may be too many control variables to learn from for the observation batches. That is why we prefer to postpone the exploration of this approach and focus instead in the present paper in the case where the dynamical system is homogeneous. As discussed in the introduction, this implies that the surrogate model parameters could and should be chosen as global. If this may avoid the underdetermination hardship, this opens up to the intricate problem of the joint localization of the state variables and global parameters.

This important issue has been studied previously in [2, 24, 32]. Their authors have proposed to make the global parameters local in the DL update step, followed by a spatial averaging of the local updated parameters to form the global parameters and be able to propagate the ensemble using these updated global parameters. By contrast, CL was chosen in [36, 46], and localization was not applied in the global parameter space. Indeed, it is difficult to choose a priori any correlation structure for the global parameters among themselves. Furthermore, it can be argued for the state/parameter covariances, that a global parameter should statistically be equally correlated to all state variables. Nonetheless, a tapering coefficient could be used for the state/parameter covariances. Ruckstuhl and Janjić [46] empirically chose N_x^{-1} as tapering coefficient, and argue that this could make the localization matrix positive semi-definite (and hence a genuine correlation matrix). Hereafter, we choose to work with the latter approach where there is no localization in parameter space but a tapering can be applied to the state/parameter covariances.

3.2.2. Covariance localization. In this section, we focus on the analysis at time t_k and therefore we drop the time index k for clarity. The ensemble mean $\bar{\mathbf{z}}$ and the normalized perturbation matrix \mathbf{X} of the ensemble $\{\mathbf{z}_i\}_{i=1,\dots,N_e}$ are defined by

$$\bar{\mathbf{z}} = \frac{1}{N_e} \sum_{i=1}^{N_e} \mathbf{z}_i, \quad \mathbf{X} = \begin{bmatrix} \frac{\mathbf{z}_1 - \bar{\mathbf{z}}}{\sqrt{N_e - 1}} & \frac{\mathbf{z}_2 - \bar{\mathbf{z}}}{\sqrt{N_e - 1}} & \cdots & \frac{\mathbf{z}_{N_e} - \bar{\mathbf{z}}}{\sqrt{N_e - 1}} \end{bmatrix}. \quad (6)$$

Let us split the background error covariances of \mathbf{z} according to the state and parameter subspaces:

$$\mathbf{B} = \begin{bmatrix} \mathbf{B}_{xx} & \mathbf{B}_{xp} \\ \mathbf{B}_{px} & \mathbf{B}_{pp} \end{bmatrix}. \quad (7)$$

We assume that \mathbf{B} has already been localized. One would typically write $\mathbf{B} = \mathbf{C} \circ (\mathbf{X}\mathbf{X}^\top)$ where \circ is the Schur product and \mathbf{C} is an admissible localization matrix, which can be written block-wise

$$\mathbf{C} = \begin{bmatrix} \mathbf{C}_{xx} & \mathbf{C}_{xp} \\ \mathbf{C}_{px} & \mathbf{C}_{pp} \end{bmatrix}. \quad (8)$$

In particular, this implies that \mathbf{B}_{xx} must be invertible. Given that the parameters are not observed, the state and parameter update reads:

$$\bar{\mathbf{x}}^a = \bar{\mathbf{x}}^f + \mathbf{B}_{xx} \mathbf{H}^\top (\mathbf{R} + \mathbf{H} \mathbf{B}_{xx} \mathbf{H}^\top)^{-1} (\mathbf{y} - \mathbf{H} \bar{\mathbf{x}}^f), \quad (9a)$$

$$\bar{\mathbf{p}}^a = \bar{\mathbf{p}}^f + \mathbf{B}_{px} \mathbf{H}^\top (\mathbf{R} + \mathbf{H} \mathbf{B}_{xx} \mathbf{H}^\top)^{-1} (\mathbf{y} - \mathbf{H} \bar{\mathbf{x}}^f). \quad (9b)$$

Let us note that the parameter update can be written as

$$\bar{\mathbf{p}}^a = \bar{\mathbf{p}}^f + \mathbf{B}_{px} \mathbf{B}_{xx}^{-1} (\bar{\mathbf{x}}^a - \bar{\mathbf{x}}^f), \quad (10)$$

which confirms that, given that the parameters are not observed, their update can be computed by a simple linear regression from the state update, using the prior statistics. In practice, one first solves the system $\mathbf{B}_{xx} \boldsymbol{\delta} = \bar{\mathbf{x}}^a - \bar{\mathbf{x}}^f$ for $\boldsymbol{\delta} \in \mathbb{R}^{N_x}$, and then computes $\bar{\mathbf{p}}^a = \bar{\mathbf{p}}^f + \mathbf{B}_{px} \boldsymbol{\delta}$. The system can be solved with a linear solver without having to explicitly compute the Schur product of \mathbf{B}_{xx} (see, e.g., [23]).

The perturbation update based on CL has the theoretical form [48]:

$$\mathbf{X}^a = \left(\mathbf{I} + \mathbf{B} \boldsymbol{\Theta}^\top \mathbf{R}^{-1} \boldsymbol{\Theta} \right)^{-\frac{1}{2}} \mathbf{X}^f, \quad (11)$$

where \mathbf{I} is the identity matrix, and $\boldsymbol{\Theta}$ stands for the tangent linear of the augmented observation operator used in (4). A careful definition of the square root matrix used in this formula can be found, e.g., in Section 2.3.1 of [11]. This update can in practice be computed resorting to augmented ensemble techniques [5, 23], which is of special interest for the assimilation of nonlocal observations. Equation (11) can be expanded into state and parameter blocks. We define $\mathbf{X}_x \in \mathbb{R}^{N_x \times N_e}$ and $\mathbf{X}_p \in \mathbb{R}^{N_p \times N_e}$ as the state and parameter block matrices of \mathbf{X} , respectively, i.e. the state and parameter normalized perturbations matrices. Then expanding (11) and using (25) in [7], we obtain

$$\mathbf{X}^a = \begin{bmatrix} (\mathbf{I} + \mathbf{B}_{xx} \boldsymbol{\Omega})^{-\frac{1}{2}} \mathbf{X}_x^f \\ \mathbf{X}_p^f - \mathbf{B}_{px} \boldsymbol{\Omega} \left(\mathbf{I} + \mathbf{B}_{xx} \boldsymbol{\Omega} + (\mathbf{I} + \mathbf{B}_{xx} \boldsymbol{\Omega})^{\frac{1}{2}} \right)^{-1} \mathbf{X}_x^f \end{bmatrix}, \quad (12)$$

with the notation $\boldsymbol{\Omega} = \mathbf{H}^\top \mathbf{R}^{-1} \mathbf{H}$. The first block, i.e. \mathbf{X}_x^a of (12) can be computed using an augmented ensemble technique. Using (25) in [7], it can be shown that \mathbf{X}_p^a can also be written:

$$\begin{aligned} \mathbf{X}_p^a &= \mathbf{X}_p^f - \mathbf{B}_{px} \mathbf{B}_{xx}^{-1} \mathbf{B}_{xx} \boldsymbol{\Omega} \left(\mathbf{I} + \mathbf{B}_{xx} \boldsymbol{\Omega} + (\mathbf{I} + \mathbf{B}_{xx} \boldsymbol{\Omega})^{\frac{1}{2}} \right)^{-1} \mathbf{X}_x^f \\ &= \mathbf{X}_p^f + \mathbf{B}_{px} \mathbf{B}_{xx}^{-1} \left\{ (\mathbf{I} + \mathbf{B}_{xx} \boldsymbol{\Omega})^{-\frac{1}{2}} - \mathbf{I} \right\} \mathbf{X}_x^f \\ &= \mathbf{X}_p^f + \mathbf{B}_{px} \mathbf{B}_{xx}^{-1} (\mathbf{X}_x^a - \mathbf{X}_x^f). \end{aligned} \quad (13)$$

Hence the updated perturbations of the parameters can be obtained by a linear regression using the prior statistics, with the updated state perturbations. Hence,

computing (13) alternately consists of (i) solving the linear system $\mathbf{B}_{xx}\Delta = \mathbf{X}_x^a - \mathbf{X}_x^f$ for $\Delta \in \mathbb{R}^{N_x \times N_e}$ and (ii) computing $\mathbf{X}_p^a = \mathbf{X}_p^f + \mathbf{B}_{px}\Delta$.

The update in parameter space can conveniently be summarized using the ensemble blocks. The ensemble matrix $\mathbf{E} = [\mathbf{z}_1 \ \mathbf{z}_2 \ \cdots \ \mathbf{z}_{N_e}]$ is decomposed into $[\mathbf{E}_x^\top \ \mathbf{E}_p^\top]^\top$ for the state and parameter ensembles. The mean state and perturbations update for the parameters can then be compactly written:

$$\mathbf{E}_p^a = \mathbf{E}_p^f + \mathbf{B}_{px}\mathbf{B}_{xx}^{-1}(\mathbf{E}_x^a - \mathbf{E}_x^f), \quad (14)$$

which can be computed (i) solving the linear system $\mathbf{B}_{xx}\Delta = \mathbf{E}_x^a - \mathbf{E}_x^f$ and (ii) updating $\mathbf{E}_p^a = \mathbf{E}_p^f + \mathbf{B}_{px}\Delta$.

As a conclusion, for an LEnKF-ML based on CL, one would first (i) update the state space part of the ensemble and then (ii) update the parameter space part of the ensemble using the state ensemble incremental update $\mathbf{E}_x^a - \mathbf{E}_x^f$ and (14) with $\mathbf{B}_{xx} = \mathbf{C}_{xx} \circ (\mathbf{X}_x^f (\mathbf{X}_x^f)^\top)$ and $\mathbf{B}_{px} = \zeta \mathbf{X}_p^f (\mathbf{X}_x^f)^\top$, where ζ is the tapering state/parameter coefficient.

3.2.3. Domain localization. There are several variants of DL [30, 41]. In this section, we use the algorithm of the local ETKF (LETKF) as formalized in [33], with most of its matrix algebra performed in ensemble space. We describe what could be the implementation of a local EnKF-ML based on the LETKF algorithm and global parameters.

Let us define the observation anomaly: $\mathbf{Y} = \Theta \mathbf{X}^f = \mathbf{H} \mathbf{X}_x^f$, where Θ, \mathbf{H} are the tangent linear of the observation operators introduced in (4). They can alternatively be computed with the secant method using the ensemble and the nonlinear operators. The state and parameter update (9), but where \mathbf{B} corresponds now to the raw sample covariance matrix (i.e. without tapering), becomes

$$\bar{\mathbf{x}}^a = \bar{\mathbf{x}}^f + \mathbf{X}_x^f \mathbf{w}^a, \quad \mathbf{w}^a = (\mathbf{I} + \mathbf{Y}^\top \mathbf{R}^{-1} \mathbf{Y})^{-1} \mathbf{Y}^\top \mathbf{R}^{-1} (\mathbf{y} - \mathbf{H} \bar{\mathbf{x}}^f), \quad (15a)$$

$$\bar{\mathbf{p}}^a = \bar{\mathbf{p}}^f + \mathbf{X}_p^f \mathbf{w}^a. \quad (15b)$$

While it is clear that (15a) can be implemented as a traditional LETKF state update, a local domain implementation of (15b) is pointless. Indeed, \mathbf{X}_p^f has no connection to state space so that one would not know how to apply a local weight update of \mathbf{w}^a to it.

Let us assume $\text{rank}(\mathbf{X}_x^f) \leq N_x$ which is a realistic assumption for the LEnKF-ML, and almost always coincides with the condition $N_e \leq N_x + 1$. In this case, \mathbf{X}_x^f has a left inverse $(\mathbf{X}_x^f)^\dagger$, i.e. $(\mathbf{X}_x^f)^\dagger \mathbf{X}_x^f = \mathbf{I}$. Then, (15b) can be transformed into

$$\bar{\mathbf{p}}^a = \bar{\mathbf{p}}^f + \mathbf{X}_p^f (\mathbf{X}_x^f)^\dagger \mathbf{X}_x^f \mathbf{w}^a = \bar{\mathbf{p}}^f + \mathbf{X}_p^f (\mathbf{X}_x^f)^\dagger (\bar{\mathbf{x}}^a - \bar{\mathbf{x}}^f). \quad (16)$$

With DL enforced, $\mathbf{X}_x^f \mathbf{w}^a$ in (15a) is computed following the traditional LETKF and $\bar{\mathbf{x}}^a$ appearing in (16) corresponds to the LETKF state update.

As for the perturbation update, the right-transform update is:

$$\mathbf{X}^a = \mathbf{X}^f (\mathbf{I} + \mathbf{Y}^\top \mathbf{R}^{-1} \mathbf{Y})^{-\frac{1}{2}}, \quad (17)$$

for the augmented state and can be expanded as

$$\mathbf{X}_x^a = \mathbf{X}_x^f (\mathbf{I} + \mathbf{Y}^\top \mathbf{R}^{-1} \mathbf{Y})^{-\frac{1}{2}}, \quad (18a)$$

$$\mathbf{X}_p^a = \mathbf{X}_p^f (\mathbf{I} + \mathbf{Y}^\top \mathbf{R}^{-1} \mathbf{Y})^{-\frac{1}{2}}. \quad (18b)$$

The DL LEnKF-ML state perturbation update as given by (18a) hence follows the traditional LETKF state perturbation update. As for the parameter perturbation update, (18b) can be written (still assuming $N_e \leq N_x + 1$):

$$\mathbf{X}_p^a = \mathbf{X}_p^f (\mathbf{X}_x^f)^\dagger \mathbf{X}_x^f (\mathbf{I} + \mathbf{Y}^\top \mathbf{R}^{-1} \mathbf{Y})^{-\frac{1}{2}} = \mathbf{X}_p^f (\mathbf{X}_x^f)^\dagger \mathbf{X}_x^a, \quad (19)$$

where \mathbf{X}_x^a has been obtained using the LETKF perturbation update.

Similarly to CL, it is then straightforward to show from Eqs. (16, 19) that those results can be summarized into a compact ensemble update formula for the parameters:

$$\mathbf{E}_p^a = \mathbf{E}_p^f + \mathbf{X}_p^f (\mathbf{X}_x^f)^\dagger (\mathbf{E}_x^a - \mathbf{E}_x^f), \quad (20)$$

where \mathbf{E}_x^a has been obtained from the ensemble update of the traditional LETKF. This could be computed by first solving the over-constrained linear system $\mathbf{X}_p^f \mathbf{\Delta} = \mathbf{E}_x^a - \mathbf{E}_x^f$ and then computing $\mathbf{E}_p^a = \mathbf{E}_p^f + \mathbf{X}_p^f \mathbf{\Delta}$. Finally, note that it is possible to taper the state/parameter error covariances and modify (20) into

$$\mathbf{E}_p^a = \mathbf{E}_p^f + \zeta \mathbf{X}_p^f (\mathbf{X}_x^f)^\dagger (\mathbf{E}_x^a - \mathbf{E}_x^f), \quad (21)$$

where ζ is the tapering coefficient. This would make sense to do so in the DL context since such tapering has not been accounted for yet in the algorithm.

More generally, this two-step DL-based EnKF with global parameters can be seen as an efficient alternative to the approach of [2, 24, 32], without the approximate averaging step. As a downside, one must carefully choose the tapering coefficient ζ .

3.2.4. Tapering of the state/parameter covariances. In this section, arguments are given for the use of a tapering coefficient of the state/parameter covariances. We follow the discussion of [46] in their Section 3.1, and slightly generalize their derivation. The main argument of [46] is that the localization matrix \mathbf{C} should be positive definite. We note, however, that this is a sufficient condition for the regularized \mathbf{B} to be positive definite, not a necessary condition. In contrast to [46], all parameters are considered here. We have $\mathbf{C}_{xx} = \boldsymbol{\rho}$, the localization matrix in state space, which is assumed to be positive definite. As explained above, we choose not to apply localization in parameter space, such that $\mathbf{C}_{pp} = \mathbf{\Pi}_{pp}$, the matrix full of 1 of size $N_p \times N_p$. The cross state/parameter correlations which accounts for the tapering reads $\mathbf{C}_{px} = \mathbf{C}_{xp}^\top = \zeta \mathbf{\Pi}_{px}$ where $\mathbf{\Pi}_{px}$ is the matrix full of 1 of size $N_p \times N_x$. Since $\mathbf{C}_{xx} = \boldsymbol{\rho} > \mathbf{0}$ is positive definite ($>$ stands for the Loewner order of symmetric matrices), the full localization matrix \mathbf{C} is positive definite if and only if the following Schur complement \mathbf{S} is positive definite (Theorem 7.7.7 in [29]):

$$\mathbf{S} = \mathbf{C}_{pp} - \mathbf{C}_{px} \mathbf{C}_{xx}^{-1} \mathbf{C}_{xp} = \mathbf{\Pi}_{pp} - \zeta^2 \mathbf{\Pi}_{px} \boldsymbol{\rho}^{-1} \mathbf{\Pi}_{xp} > \mathbf{0}, \quad (22)$$

where $\mathbf{\Pi}_{xp} = \mathbf{\Pi}_{px}^\top$. Note that Ruckstuhl and Janjić [46] chose to consider the other Schur complement defined in state subspace. For any $\mathbf{p} \in \mathbb{R}^{N_p}$, we have

$$\mathbf{p}^\top \mathbf{S} \mathbf{p} = \sigma^2 (1 - \zeta^2 \mathbf{1}^\top \boldsymbol{\rho}^{-1} \mathbf{1}), \quad (23)$$

where $\sigma = \sum_{i=1}^{N_e} p_i$ and $\mathbf{1} = [1 \ 1 \ \dots \ 1]^\top \in \mathbb{R}^p$. If $\lambda_{\min} > 0$ is the smallest eigenvalue of the positive definite $\boldsymbol{\rho}$, we have

$$\mathbf{p}^\top \mathbf{S} \mathbf{p} \geq \sigma^2 (1 - \zeta^2 N_x \lambda_{\min}). \quad (24)$$

Hence, a necessary condition for \mathbf{S} , and hence \mathbf{C} , to be positive semi-definite is

$$\zeta < \sqrt{\frac{\lambda_{\min}}{N_x}}. \quad (25)$$

For a homogeneous regular (non-random) positive ρ , λ_{\min} is expected to scale like N_x^{-1} . Hence, from (25) an upper bound for ζ should scale like $g(N_e)/N_x$ with increasing N_x . The choice $\zeta = N_x^{-1}$ was astutely proposed on empirical grounds in [46].

3.3. The iterative ensemble Kalman filter. Developing a local EnKF-ML is certainly the most critical task for the scalability of the approach. By contrast, developing an iterative EnKF-ML is of theoretical interest, in particular when the time interval between update is large enough so that the nonlinearity of the true model significantly emerges. In such circumstances, the performance of the EnKF degrades and it has to be replaced by its iterative variant, the IEnKF [50, 13]. An IEnKF-ML is an intriguing subject, because the nonlinear dynamical system has to be estimated along with the state trajectory. Joint state and parameter estimation with an IEnKF was explored in [14], but the parameters were only constraining the linear part of the dynamics. The IEnKF was used to retrieve boundary conditions of a computational fluid dynamics problem in [19], but the dynamics were assumed stationary.

In an IEnKF-ML, not only is state augmentation used as in the EnKF-ML but, by contrast, it is also optimized on in the analysis step of the method which is of variational nature. For the sake of simplicity, we will not use localization with the IEnKF-ML, although localized variants are possible (see [7, 49]). The cost function that underlies the analysis of the IEnKF-ML is defined over a lag-one DA window (DAW) $[t_0, t_1]$.

Because the surrogate model is likely to be flawed, especially in the first cycles of the (I)EnKF-ML sequential runs, model error should be accounted for, either by multiplicative inflation or by addition of stochastic noise on the state. Hence, a natural framework for the IEnKF-ML is the IEnKF-Q [49], i.e. an IEnKF that rigorously accounts for additive model error. The IEnKF-ML cost function, based on the generalization of both the cost function (4) of the EnKF-ML and the cost function of the IEnKF-Q defined in (2b) of [49], reads

$$\mathcal{J}(\mathbf{z}_0, \mathbf{z}_1) = \frac{1}{2} \|\mathbf{y}_1 - \boldsymbol{\Theta}_1(\mathbf{z}_1)\|_{\mathbf{R}_1^{-1}}^2 + \frac{1}{2} \|\mathbf{z}_1 - \mathcal{M}_0(\mathbf{z}_0)\|_{\boldsymbol{\Xi}_1^{-1}}^2 + \frac{1}{2} \|\mathbf{z}_0 - \bar{\mathbf{z}}_0^f\|_{\mathbf{B}_0^{-1}}^2, \quad (26)$$

where

$$\mathcal{M}_0(\mathbf{z}_0) = \begin{bmatrix} \mathbf{F}^0(\mathbf{z}_0) \\ \mathbf{p}_0 \end{bmatrix} \quad (27)$$

with $\mathbf{F}^0(\mathbf{z}_0)$ standing for $\mathbf{F}^0(\mathbf{p}_0, \mathbf{x}_0)$, and assuming the persistence model for the surrogate model parameters. Note that depending on the definition of the model noise statistics $\boldsymbol{\Xi}_1$, stochastic perturbations are also possible for the propagation of the surrogate model parameters, even though the deterministic parameter evolution model is persistence.

Thanks to the augmented state trick, (26) has exactly the same form as that of the IEnKF-Q, so that we closely follow the derivation of its analysis step. We introduce the state model perturbation matrix as $\mathbf{X}_1^q \in \mathbb{R}^{N_z \times N_q}$ and it is defined through $\boldsymbol{\Xi}_1 = \mathbf{X}_1^q (\mathbf{X}_1^q)^\top$, where N_q is the number of centered model error perturbations. Sakov et al. [49] discussed of the relevance of this factorization. The cost function can be written in ensemble space through the parameterization:

$$\mathbf{z}_0 = \bar{\mathbf{z}}_0^f + \mathbf{X}_0 \mathbf{w}_z, \quad (28a)$$

$$\mathbf{z}_1 = \mathcal{M}_0(\mathbf{z}_0) + \mathbf{X}_1^q \mathbf{w}_q. \quad (28b)$$

Denoting $\mathbf{w} = [\mathbf{w}_z^\top \quad \mathbf{w}_q^\top]^\top \in \mathbb{R}^{N_e + N_q}$ and following [49], we obtain a very compact cost function in ensemble space:

$$\mathcal{J}(\mathbf{w}) = \frac{1}{2} \|\mathbf{y}_1 - \boldsymbol{\Theta}_1(\mathbf{z}_1)\|_{\mathbf{R}_1^{-1}}^2 + \frac{1}{2} \|\mathbf{w}\|^2, \quad (29)$$

under the constraints (28). Because it has the same mathematical structure as (8) of [49], the algorithm of the IEnKF-ML is formally the same as that of the IEnKF-Q, see Algorithm 1 of [49], with the state vectors being replaced with state/parameter augmented vectors.

Note that, for the sake of simplicity, we could choose $\boldsymbol{\Xi}_1^{-1}$ to be of the form:

$$\boldsymbol{\Xi}_1^{-1} = \begin{pmatrix} \mathbf{Q}_1^{-1} & \mathbf{0} \\ \mathbf{0} & \mathbf{0} \end{pmatrix}, \quad (30)$$

i.e. the parameter propagation is persistence only, without additional stochastic perturbations. In that case, (26) reads

$$\mathcal{J}(\mathbf{z}_0, \mathbf{z}_1) = \frac{1}{2} \|\mathbf{y}_1 - \mathbf{H}_1(\mathbf{x}_1)\|_{\mathbf{R}_1^{-1}}^2 + \frac{1}{2} \|\mathbf{x}_1 - \mathbf{F}^0(\mathbf{z}_0)\|_{\mathbf{Q}_1^{-1}}^2 + \frac{1}{2} \|\mathbf{z}_0 - \bar{\mathbf{z}}_0^f\|_{\mathbf{B}_0^{-1}}^2, \quad (31)$$

the model error perturbation matrix becomes $\mathbf{X}_1^q \in \mathbb{R}^{N_x \times N_q}$ such that $\mathbf{Q}_1 = \mathbf{X}_1^q (\mathbf{X}_1^q)^\top$, and (28b) should read

$$\mathbf{x}_1 = \mathbf{F}^0(\mathbf{z}_0) + \mathbf{X}_1^q \mathbf{w}_q. \quad (32)$$

Finally, (29) could be re-written:

$$\mathcal{J}(\mathbf{w}) = \frac{1}{2} \|\mathbf{y}_1 - \mathbf{H}_1(\mathbf{x}_1)\|_{\mathbf{R}_1^{-1}}^2 + \frac{1}{2} \|\mathbf{w}\|^2. \quad (33)$$

We also remark that the decoupling of \mathbf{w}_z and \mathbf{w}_q when the observation operator is linear, which was put forward and explained in Section 3 of [49] and Appendix B of [25], also happens for the IEnKF-ML.

Let us now discuss two appealing properties of the IEnKF-ML, which may help scale it up to high dimensional systems.

The IEnKF is a very powerful nonlinear filtering technique. But it has a numerical cost due to the propagation of the ensemble within the DA window for each iteration of the nonlinear variational analysis. The average number of iterations can be kept quite small in a cycled DA run, as opposed to a 4D-Var, but the number of ensemble propagations may easily be twice that of a traditional EnKF. By contrast, the propagation of the ensemble within the variational analysis of the IEnKF-ML is carried out using the surrogate model, which is likely to be numerically much cheaper especially when using efficient highly-parallelised, ML libraries.

As opposed to the EnKF-ML, the adjoint of the surrogate model is explicitly or implicitly used in the IEnKF-ML. In the Algorithm 1 of [49], it is evaluated using finite-differences or the secant method, and a simple transposition in the ensemble subspace. This is the approach used in ensemble variational DA techniques (see Section 4.5 of [18]), and which was also advocated in the ML context in the absence of an adjoint model [35]. If the surrogate model is implemented in TensorFlow or Pytorch, an efficient adjoint can be obtained, and would possibly make the IEnKF-ML more accurate, especially if localized or if a static background is additionally used in the analysis. Moreover, this would avoid the need for ensemble propagations within the DA window.

4. Numerical results. In this section, we test the global and local EnKF-ML as well as the IEnKF-ML, mostly on the low-order chaotic model L96 but also on the L05III model. Both models are very commonly employed to test new DA schemes so that they are well suited for this study. The true L96 model lies in the set of all achievable surrogate models by the representation described in Section 2. Hence, the true dynamics could theoretically be reconstructed. By contrast, the true L05III model, which has two scales of motion, cannot be accurately represented by the surrogate model representation chosen in Section 2 since it only accounts for a single scale of motion (no nested submodel).

4.1. Lorenz-96. The L96 model is defined by a set of ODEs over a periodic domain with variables indexed by $n = 0, \dots, N_x - 1$:

$$\frac{dx_n}{dt} = (x_{n+1} - x_{n-2})x_{n-1} - x_n + F, \quad (34)$$

where $N_x = 40$, $x_{N_x} = x_0$, $x_{-1} = x_{N_x-1}$, $x_{-2} = x_{N_x-2}$, and $F = 8$. This model is an idealized representation of a one-dimensional latitude band of the Earth atmosphere. The dimension of the unstable and neutral subspace is $N_0 = 14$. The truth run of the L96 model is integrated using the fourth-order Runge–Kutta (RK4) scheme with a time step of $\delta t = 0.05$.

The surrogate model to be used has a one-to-one correspondence with all L96 variables $\{x_n\}_{n=0, \dots, N_x-1}$, so that it can exhaustively represent the dynamics of L96. The stencil of the surrogate model, as defined in Section 2, is chosen to be $L = 2$ (i.e. contains $2L + 1 = 5$ local variables).

4.2. Lorenz-05III. The two-scale Lorenz model L05III is given by the following two-scale set of ODEs:

$$\frac{dx_n}{dt} = \psi_n^+(\mathbf{x}) + F - h \frac{c}{b} \sum_{m=0}^9 u_{m+10n}, \quad (35a)$$

$$\frac{du_m}{dt} = \frac{c}{b} \psi_m^-(b\mathbf{u}) + h \frac{c}{b} x_{m/10}, \quad (35b)$$

$$\psi_n^\pm(\mathbf{x}) = x_{n\mp 1}(x_{\pm 1} - x_{n\mp 2}) - u_n, \quad (35c)$$

for $n = 0, \dots, N_x - 1$ with $N_x = 36$, and $m = 0, \dots, N_u - 1$ with $N_u = 360$. The indices are defined periodically over their domains and $m/10$ stands for the integer division of m by 10. The other parameters are set to their original values: $c = 10$ for the time-scale ratio, $b = 10$ for the space-scale ratio, $h = 1$ for the coupling between the scales, and $F = 10$ for the forcing. When uncoupled ($h = 0$), the dimension of the unstable and neutral subspace of the coarse modes model compartment is $N_0 = 13$ (for a thorough analysis of this dynamical system, see [17]). The stencil of the surrogate model is chosen to be $L = 2$. The vector \mathbf{u} represents unresolved scales and hence model error when only considering the slow variables \mathbf{x} . It is integrated with an RK4 scheme and the time step $\delta t = 0.005$ since it is stiffer than the L96 model.

The surrogate model has a one-to-one correspondence with the coarse scale variables $\{x_n\}_{n=0, \dots, N_x-1}$ only, so that it can only represent an approximation of the dynamics of L05III.

4.3. Objective and metric. The objective is to estimate both the state trajectory and the dynamics as a set of ODEs. For the global and local EnKF-ML, and for the IEnKF-ML, we make a selection of what we believe to be relevant and revealing experiments since this generalized DA/ML problem has many degrees of freedom in its setup, even more than typical DA experiments.

The metric is the average (over time) root mean square error of the state analysis (RMSE). We do not report a metric for the dynamics as this is not relevant for L05III and because, in such a sequential context, the fitness of the surrogate dynamics will manifest itself in the state variable RMSE. The RMSE will be averaged over several (typically 10) long data assimilation runs for the error statistics to be reliable.

For each of the DA experiments, the setup will be specified. They correspond to, or are variations of classical DA configurations for the L96 and L05III models.

4.4. The EnKF-ML. In this section, we study numerically the basic EnKF-ML, which is based on an ETKF, without either localization or nonlinear iterations. Because there are so many hyperparameters to consider such as ensemble size, frequency and sparsity of observations, inflation on the state or the parameters, model error noise on the state, etc, we have initially performed several sensitivity studies to freeze a few of these hyperparameters, hoping not to lose much in terms of accuracy of the filters in the process.

4.4.1. Sensitivity to the multiplicative inflation. We first consider a multiplicative inflation for the state variables and another for the model parameters, and compare to a filter where both inflations are equal (hence reducing the number of hyperparameters to test upon). We choose to perform $N_{\text{exp}} = 50$ identical experiments with as many different random seeds, with an ensemble size in the range $N_e = [12, 52]$ for both L96 and L05III. The L96 system is fully observed $\mathbf{H} = \mathbf{I}$ with a frequency of $\Delta t = 0.05$. The coarse variables (and only them) of the L05III system are fully observed with a frequency of $\Delta t = 0.05$. For both models, the observations are independently perturbed with a normal distribution of error covariance matrix $\mathbf{R} = \mathbf{I}$. The synthetic data assimilation runs make use of these observations only, over 10^4 time-steps, and after a burn-in of 2×10^3 time-steps. The average RMSE is computed by comparing the analysis of the DA runs with the true trajectory. Finally, we do not account for a prior model error noise in these specific experiments ($\mathbf{Q} = \mathbf{0}$).

The state variables and parameter inflations are independently varied in the *dual inflation* case, and varied but equal to each other in the *same inflation* case. The RMSEs are reported in Figure 1a, and represent the best ones over all the tested inflation(s).

In the absence of localization, the most relevant values are for N_e large enough. In this regime, we observe that the dual inflation scheme does not offer a significant advantage over the same inflation scheme, although we remark a small edge for larger N_e in the L96 case. That is why, for the sake of reducing the number of hyperparameters, the multiplicative inflation will hereafter be the same for the state variables and parameters, unless explicitly mentioned.

4.4.2. Sensitivity to prior model error noise. We then test the impact of accounting for Gaussian model errors with prior error covariance matrix $\mathbf{Q} = \sigma_q^2 \mathbf{I}$ on the state vector, using the deterministic Sqrt-CORE algorithm [44]. We opt for the setup of the previous experiment, except that N_e is now set to 40 in the L96 case, and 36 in the L05III case (where the RMSEs in Figure 1a are the best). The model error standard deviation σ_q , which parameterizes Sqrt-CORE is then varied. The

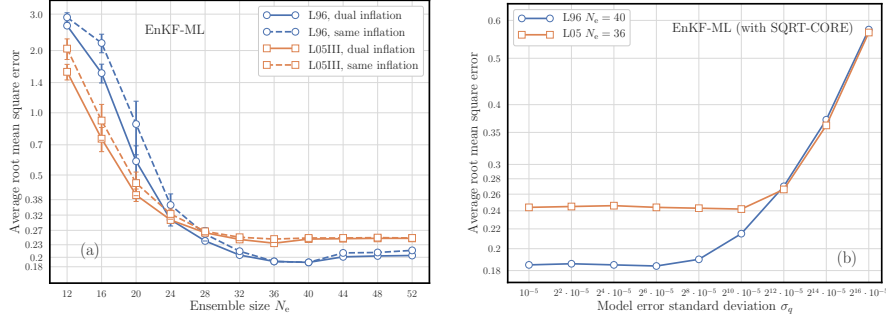


FIGURE 1. Left panel (a): For both models, comparison of two EnKF-MLs where (i) the RMSE is minimized over both state and parameter inflations (dual) and (ii) the RMSE is minimized over the same inflation for state and parameter (same). Right panel (b): For both models, dependence of the EnKF-ML RMSE on the prior model error standard deviation σ_q . The error bars correspond to the standard deviation of $N_{\text{exp}} = 50$ repeated experiments.

optimally tuned (over the inflation) RMSE as a function of σ_q is plotted in Figure 1b. We observe that the stochastic noise does not really help, even in the less identifiable case of L05III. It is likely that mitigating the impact of the surrogate model mismatch with the true dynamics is a role already played by the multiplicative inflation. Hence, we will choose $\sigma_q = 0$ for the L96 and L05III hereafter. It must however be kept in mind that this conclusion might not apply to more complex models where multiplicative inflation does not necessarily optimally compensate for model error.

4.4.3. *Accuracy as a function of the ensemble size.* With these choices for the hyperparameters, we obtain RMSE curves for the EnKF-ML and both models similar to the first experiments, still using $N_{\text{exp}} = 50$. In addition, we compare the performance with the traditional ETKF where the model is known. The results are shown in Figure 2a.

In the L96 case, the performance achieved by the EnKF-ML is as good as that of the traditional EnKF in the critical region around $N_e = 40$ (in the absence of localization). The EnKF outperforms the EnKF-ML for $N_e > 40$, probably because we use the same inflation for state variables and parameters. In the L05III case, the performance is not as good as the EnKF one. But considering that by the sole observations of the coarse modes, the true model cannot be identified, the accuracy achieved by the EnKF-ML is actually remarkable.

4.4.4. *Lyapunov exponents.* In order to numerically check the dynamical argument on the Lyapunov spectra which has consequences on localization (see Section 3.1), we compute the Lyapunov spectrum of the surrogate model around an L96 trajectory and compare it to the Lyapunov spectrum of the true L96 model. The spectra are plotted in Figure 2b and corroborate our theoretical arguments. In particular, the positive part of the spectra coincide and the surrogate model spectrum has as many neutral exponents as the number of dynamical parameters plus one because the model is autonomous. Quantitatively, we have $N_0 = 14$ and $N_p = 18$ for the

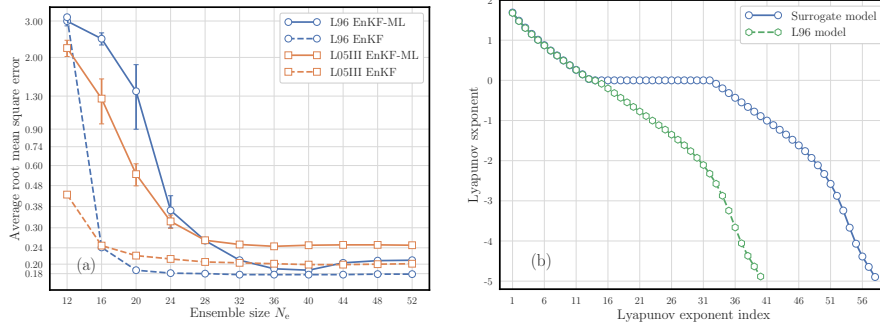


FIGURE 2. Left panel (a): For both models, comparison of the performance of the EnKF-ML where the model is unknown and of the traditional EnKF where the model is known. The error bars are obtained from the standard deviation of $N_{\text{exp}} = 50$ repeated experiments. Right panel (b): Comparison of Lyapunov spectra of the L96 model and of the surrogate model around an L96 trajectory.

L96 experiment, i.e., $N_0 + N_p = 32$, and approximately the same for the L05III experiment. Note also that for $N_e \geq N_0 + N_p + 1 = 33$, the filters accuracy has reached its close to optimal RMSE value, as predicted in Sec. 3.1.

4.4.5. Initialization of the ensemble. The success of the DA runs critically depends on the initialization of the ensemble. In all experiments, the parameter part of the initial ensemble members is obtained by multiplicative log-normal perturbations of the true model parameters in the L96 case, and of the true model parameters of the coarse modes dynamics in the L05III case. The standard deviation of the log-normal distribution is chosen to be 0.5. Moreover, a random normal noise of standard deviation 0.1 is added to these perturbations, mainly to initialize the coefficients meant to be close to zero. In spite of this rather tough initialization, we rarely observe divergences of the EnKF-ML, in spite of the first iterations of the DA runs where the surrogate model estimate is necessarily poor. A typical example of the evolution of the parameters is displayed in Figure 3 for the L96 model (where there is a one-to-one correspondence between the parameters of the true and surrogate dynamics). As expected, what seems to matter is a proper initialization of the spread of the ensemble, consistent with that of the error in initial conditions. Obviously, the initialization would have to be critically re-analyzed with more complex models, where a cold start (without any prior on the dynamics) could yield divergence.

4.5. The local EnKF-ML. In this section, we study the local EnKF-ML. For the sake of limiting the number of experiments, we focus on the LEnSRF (local ensemble square root Kalman filter) implementation only, i.e. with CL, and leave testing the LETKF-ML based on DL for future work. We use a localization matrix based on the Gaspari-Cohn piecewise rational function [26]. The time interval between updates is $\Delta t = 0.05$. Unless otherwise stated, the synthetic observations are generated in the exact same way as in Section 4.4, for both the L96 and L05III models. We do not account for prior model error ($\mathbf{Q} = \mathbf{0}$). The synthetic data

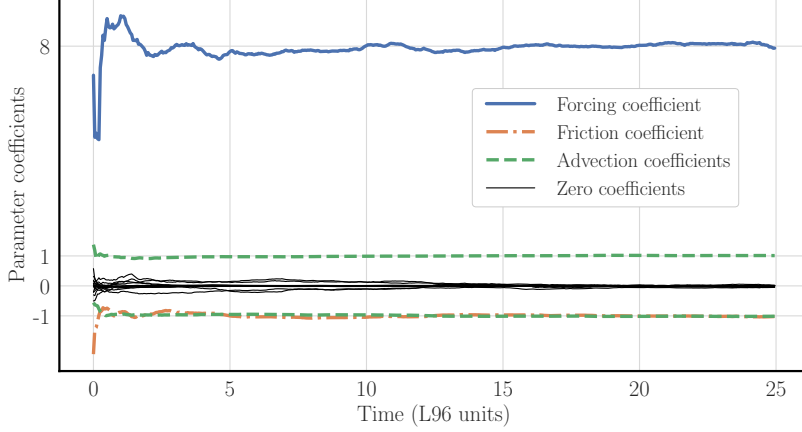


FIGURE 3. Initial evolution of the 18 parameters of the surrogate model learned on the observation of a L96 model run. The key parameters are the forcing ($F = 8$ in the true model), the friction (-1 in the true model) and the advection coefficients ($-1, 1$ in the true model).

assimilation experiments run over 10^4 time-steps, after a burn-in of 2×10^3 time-steps, and are repeated $N_{\text{exp}} = 10$ times. We compute the best average RMSE over a range of multiplicative inflations, localization lengths and of state/parameter tapering coefficients.

4.5.1. Accuracy as a function of the ensemble size. The accuracy of the LEnKF-ML is estimated via the RMSE, as a function of the ensemble size. Keep in mind that the model parameters are not localized, so that a significant ensemble size should be required for convergence even with localization. The LEnKF-ML is compared with the traditional LEnKF (in the shape of the LEnSRF here) based on the exact same setup but with the exception that the model is known. For the sake of numerical efficiency, the LEnSRF requires special attention in the L05III case, where only the coarse modes are observed, i.e. $N_x = 36$ out of $N_x + N_u = 396$ variables. The brute force implementation of the LEnSRF, (11), without augmented ensemble techniques [5, 23] becomes costly and we prefer to carry out the analysis expressed in observation space since (i) $N_y/(N_x + N_u) \ll 1$ and (ii) the observations are local. In that case, we can use (12) in [8] which is the left-transform perturbation update but with algebra in observation space. As a consequence, we resort to the following convenient update formula for the state variables:

$$\bar{\mathbf{x}}^a = \bar{\mathbf{x}}^f + \mathbf{B}_{xy}^\top (\mathbf{R} + \mathbf{B}_{yy}^\top)^{-1} (\mathbf{y} - \mathbf{H}\bar{\mathbf{x}}^f), \quad (36a)$$

$$\mathbf{X}_x^a = \mathbf{X}_x^f - \mathbf{B}_{xy} \left(\mathbf{R} + \mathbf{B}_{yy} + \mathbf{R} (\mathbf{I} + \mathbf{R}^{-1} \mathbf{B}_{yy})^{\frac{1}{2}} \right)^{-1} \mathbf{Y}, \quad (36b)$$

where $\mathbf{B}_{xy} = \mathbf{C}_{xy} \circ (\mathbf{X}\mathbf{Y}^\top)$ and $\mathbf{B}_{yy} = \mathbf{C}_{yy} \circ (\mathbf{Y}\mathbf{Y}^\top)$, using the fact that the observations are local so that the localization matrix blocks \mathbf{C}_{xy} and \mathbf{C}_{yy} can be straightforwardly defined. The subsequent parameter update step is unchanged, i.e. (14).

The results are shown in Figure 4. Since the error covariances of the parameters

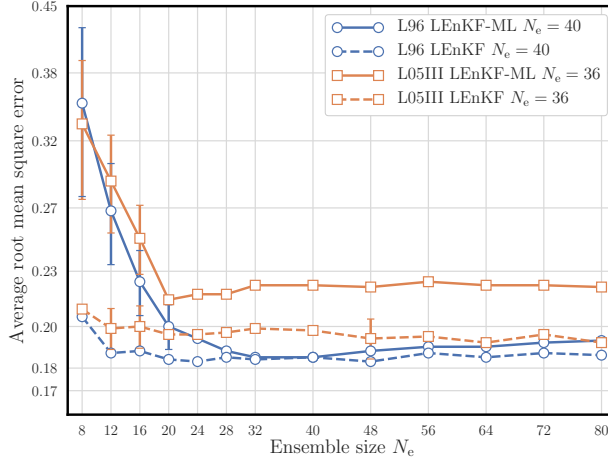


FIGURE 4. For both models, comparison of the performance of the LEnKF-ML where the model is unknown and of the traditional LEnKF where the model is known. The error bars are obtained from the standard deviation of $N_{\text{exp}} = 10$ repeated experiments.

are not regularized, we can surmise that the LEnKF-ML should be efficient for an ensemble size beyond N_p plus a few additional members meant to deal with spatial state extension and on which localization applies, typically 5 for both model cases. Hence the filter should reach good accuracy for $N_e \geq N_p + 5 + 1 = 24$, which is indeed what can be observed in Figure 4. Like for the global EnKF-ML, the accuracy in the L96 case reaches that of the traditional EnKF, while it is slightly degraded compared to the traditional EnKF in the L05III case because of its non-identifiability when only the coarse modes are represented.

With the traditional LEnKF applied to the L96 model, an ensemble size of 5 to 8 with the above setup is sufficient to reach a good accuracy, while we need $N_e \gtrapprox 24$ for the LEnKF-ML, which questions its scalability. To make sure that the LEnKF-ML is spatially scalable while keeping a good accuracy, we perform the experiment with the same setup as before but with an ensemble size of $N_e = 40$, a localization length of 18 (defined as half-length of the Gaspari–Cohn function), an inflation of 1.005 and the state space dimension of the L96 model is varied from $N_x = 80$ to $N_x = 1020$. Ensemble size, localization length and inflation are fixed since we believe they are intensive quantities (as opposed to extensive). As hoped for, the average RMSE remains within the interval $[0.186, 0.190]$ with a standard deviation of 3×10^{-3} for $N_x = 80$ down to 5×10^{-4} for $N_x = 1020$. We conclude that the LEnKF-ML is indeed scalable.

4.5.2. Sensitivity to the observation density and observation noise magnitude. In this section, we study the impact of the observation density N_y/N_x on the accuracy of LEnKF-ML, compared to the traditional LEnKF. At each data assimilation cycle, N_y random grid points out of N_x (out of N_x coarse modes for L05III) are observed. In a second experiment, we study the impact of the observation error standard deviation σ_y , assuming $\mathbf{R} = \sigma_y^2 \mathbf{I}$, on the accuracy of LEnKF-ML, compared to the

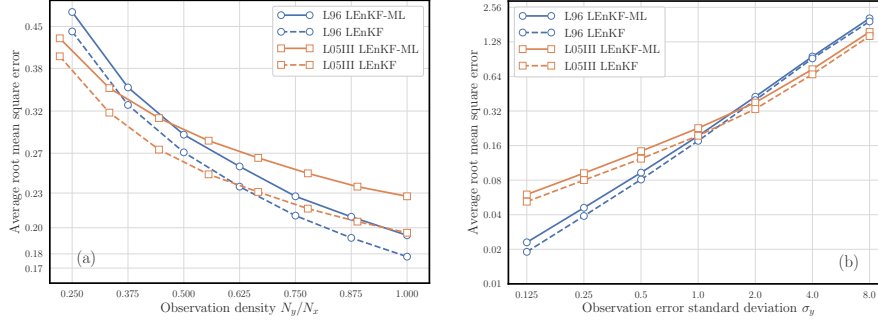


FIGURE 5. Left panel (a): For both models, comparison of the performance of the LEnKF-ML where the model is unknown and of the traditional LEnKF where the model is known, as a function of the observation density. Right panel (b): For both models, comparison of the performance of the LEnKF-ML where the model is unknown and of the traditional LEnKF where the model is known, as a function of the observation error standard deviation. In all cases, the ensemble size is $N_e = 24$ and the RMSE statistics are accumulated over $N_{\text{exp}} = 10$ experiments.

traditional LEnKF, when all N_x grid points are observed (all the coarse modes in the L05III case). In both experiments, the ensemble size is set to $N_e = 24$.

Those are classical tests to evaluate DA techniques; they are needed here since standard ML techniques are designed for fully and accurately observed systems. The results are reported in Figure 5. The figure displays the best average RMSEs over a range of localization lengths, tapering coefficients and multiplicative inflations. They all show good performance of the LEnKF-ML filters for a wide range of hyperparameters (N_y/N_x and σ_y). It is noticeable that, in relative terms (the y-axis of both panels are in logarithmic scale), the LEnKF-ML catches up with the traditional LEnKF reference as the DA conditions become more dire (less observations, more noise).

4.5.3. Optimal state/parameter tapering as a function of the ensemble size and state space dimension. One intriguing problem is to determine the proper scaling of the optimal parameter/state tapering coefficient ζ with the ensemble size N_e and the state space dimension N_x . Is the tapering of the cross state/parameter covariances a genuine regularization based on prior assumptions of these specific covariances, like traditional localization is? Is it just a mathematical requirement for the regularized covariance matrices to be semi-positive definite? Or is it an adjustment coefficient that tune the increment in parameter space as is clear from the update formula (21) and briefly alluded to in [36]?

The optimal tapering coefficient ζ is computed in the L96 model case only (for the sake of simplicity), using the LEnKF-ML. Its dependence on the ensemble size at fixed model dimension $N_x = 40$ is studied. Its dependence on the model dimension is then computed, while keeping the ensemble size fixed ($N_e = 40$), using a fixed joint multiplicative inflation of 1.005 and a localization length of 18, since these optimal intensive hyperparameters should not change significantly with the state space dimension. The results are reported in Figure 6.

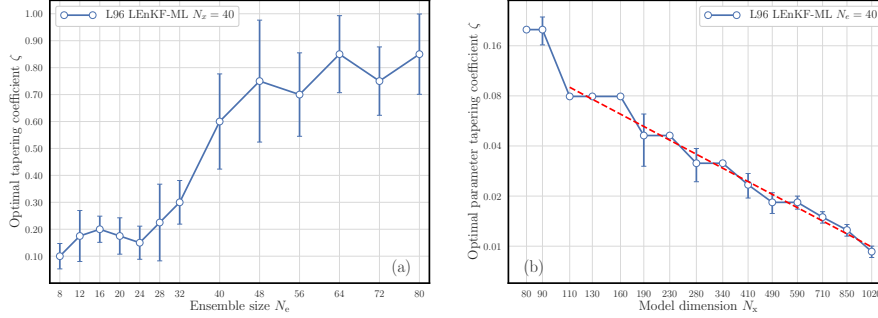


FIGURE 6. Left panel (a): Optimal tapering coefficient ζ across a range of ensemble sizes N_e for LEnKF-ML applied to the L96 model ($N_x = 40$). Right panel (b): Optimal tapering coefficient ζ across a range of model state space dimensions N_x for LEnKF-ML applied to the L96 model, assuming $N_e = 40$, a fixed multiplicative inflation and localization length. The error bars are obtained from the standard deviation of $N_{\text{exp}} = 10$ repeated experiments.

At fixed state space dimension, the sampling errors in the full covariance matrices vanish, as the ensemble size increases. Indeed, as can be seen in Figure 6a, the optimal ζ increases towards 1 and saturates at higher value (≥ 0.70) for $N_e \geq 48$. It was conjectured in [46] and in our Section 3.2.4 that the optimal ζ may asymptotically scale like the inverse of the dimension of state space. This is indeed what is observed in Figure 6b. Asymptotically, i.e. for large enough state space dimension (here we have chosen $N_x \geq 110$), the optimal ζ scales like $N^{-\alpha}$, where $\alpha = 0.99 \pm 0.05$, as illustrated by the fit dashed red line in Figure 6b.

4.6. The iterative EnKF-ML. For testing the iterative EnKF-ML, we do not consider localization since it would further add complexity. However, there is no fundamental obstacle to using localization in a stronger nonlinearity context, although (i) it is more intricate than in the traditional EnKF context with a weaker nonlinearity (see [7, 49]), (ii) the techniques developed in Section 3.2 to consider global parameters and local variables should be implemented. For evaluating the IEnKF-ML scheme, we use the same fully observed setup as before. The ensemble size is chosen to be $N_e = 40$ and $N_e = 36$ for the L96 and L05III cases, respectively. The interval time between updates is varied uniformly from $\Delta t = 0.05$ to $\Delta t = 0.60$, which allows to increase the nonlinearity of the problem, in a regime where the iterative filters very significantly outperform the non-iterative filters. This is a classical setup for testing IEnKF methods [50]. However, as opposed to all the experiments considered so far in this paper, we re-instate back dual inflation for state variables and parameters, and we consider the possibility of accounting for additive model error with a normal noise of error covariance matrix $\mathbf{Q} = \sigma_q^2 \mathbf{I}$. It is adequate to do so since the surrogate model is propagated over much larger time intervals, and might be subject to a lot of model error and biases. Considering additive model noise is also part of the IEnKF-Q from which the IEnKF-ML is directly inspired. As control variable of the analysis step of the IEnKF-Q and now IEnKF-ML, this error is not implemented with SQRT-CORE which may have been employed in the (L)EnKF-ML.

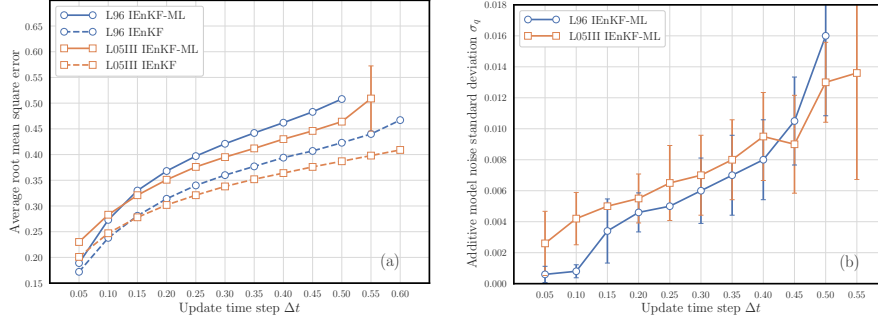


FIGURE 7. Left panel (a): Comparison for both models of the performance of the IEnKF-ML where the model is unknown and of the traditional LEnKF where the model is known, as a function of the time interval between updates Δt . Right panel (b): Optimal additive model noise standard deviation σ_q , a parameter of the IEnKF-ML as a function of the time interval between updates Δt , for both model cases. The absence of a point means that at least of the $N_e = 10$ DA run was divergent. The error bars are obtained from the standard deviation of $N_{\text{exp}} = 10$ repeated experiments.

In Figure 7a, we report the best RMSEs over the inflation and model error noise standard deviation σ_q , for both model cases. These accuracy results are compared in each case to the traditional IEnKF where the model is perfectly known. As expected, there is quite an RMSE gap between the performance of the IEnKF-ML and the traditional IEnKF schemes. However, the IEnKF-ML yields RMSEs significantly lower than the EnKF-ML or even the traditional EnKF for large enough Δt (not shown, see [13], their Figure 3). Moreover, they are stable up to large values of Δt , 0.50 in the L96 case and 0.55 in the L05III case. The optimal σ_q , which corresponds to the lowest RMSE, is plotted in Figure 7b, and shows a steady increase as Δt is increased, as could be expected. Note that this hyperparameter competes with the inflation applied to model parameters, which also steadily increases with Δt (not shown).

5. Conclusion. In this paper, we have studied the possibility to learn not only the state of a physical system from its partial and noisy observation, as in traditional DA, but also its full dynamics. This requires to use a parametric although quite general representation of the dynamics, such as a residual neural network implemented using a machine learning library. We have extended the traditional EnKF, local EnKF and iterative EnKF to their machine learning counterparts where the model dynamics are learned. This is achieved sequentially, by successive updates as observation batches are collected. These schemes are based on augmented state/parameter vectors and are hence strongly connected to state/parameter EnKF estimation. The LEnKF-ML depends on the symmetries of the dynamics. When the dynamics are homogeneous, the model representation parameters are global, as opposed to the state vector, and we developed an efficient two-step approach for updating the LEnKF-ML. Localization is not applied to the global parameters but a tapering of the parameter/state variable cross covariances is necessary. On dynamical system grounds, it was explained that the ensemble size should be large enough

to represent the local degrees of freedom of the state vector (as in traditional DA) and the global model parameters. In this case, the model representation should be minimal, typically a few dozens of parameters to efficiently represent homogeneous one or two-dimensional dynamics. The IEnKF-ML is a surprisingly simple generalization of the traditional IEnKF, albeit in augmented state/parameter space. Note, however, that the parameters are not only estimated through the cross-covariances with the observed state compartment, but also through the implicit nonlinear variational analysis of the IEnKF-ML. Because the sensitivities required by the analysis are generated by surrogate model propagations, the IEnKF-ML may turn much faster than the usual IEnKF if efficient ML libraries are used.

A selection of these algorithms were numerically tested on the L96 model where the dynamics can theoretically be identified through an appropriate set of parameters, and the two-scale L05III model where only the coarse modes are observed and represented so that the true model cannot be accurately represented by the surrogate model. All tests were successful with good RMSEs typically 5 – 10% and 5 – 15% higher than with their traditional counterpart where the dynamics are exactly known, respectively.

From this point on, there are many potential subjects of investigation. Let us mention a few specific ones, among many. First of all, we did not numerically evaluate the LETKF-ML, the DL counterpart to the LEnSRF-ML, although we describe the algorithmic parameter update step. We plan on doing so. Next, we would like to investigate the LEnKF with an inhomogeneous dynamics where not only the state but the model parameters are also local. Such LEnKF-ML is also scalable, and should not require much larger ensembles. Third, in this paper, we have only focused on the filtering aspects of these online schemes. But we could also consider sequential fixed-lag smoothers to better learn autonomous or slowly varying dynamics. Extending the EnKF-ML to classical smoother would yield the EnKS-ML and extending the IEnKF-ML to longer DA time window would yield the IEnKS-ML. We do not anticipate further theoretical complications other than those mentioned in this paper. We hope that this could significantly help in improving the accuracy of the surrogate dynamics.

Acknowledgments. The authors acknowledge many insightful discussions on related topics with our colleagues Julien Brajard, Massimo Bonavita, Alberto Carrassi, Patrick Laloyaux, and Laurent Bertino. CERE is a member of Institut Pierre-Simon Laplace (IPSL).

REFERENCES

- [1] H. D. I. Abarbanel, P. J. Rozdeba and S. Shirman, Machine learning: Deepest learning as statistical data assimilation problems, *Neural Computation*, **30** (2018), 2025–2055.
- [2] A. Aksoy, F. Zhang and J. Nielsen-Gammon, Ensemble-based simultaneous state and parameter estimation in a two-dimensional sea-breeze model, *Mon. Wea. Rev.*, **134** (2006), 2951–2969.
- [3] T. Arcomano, I. Szunyogh, J. Pathak, A. Wikner, B. R. Hunt and E. Ott, A machine learning-based global atmospheric forecast model, *Geophys. Res. Lett.*, **47** (2020), e2020GL087776.
- [4] C. H. Bishop, B. J. Etherton and S. J. Majumdar, Adaptive sampling with the ensemble transform Kalman filter. Part I: Theoretical aspects, *Mon. Wea. Rev.*, **129** (2001), 420–436.
- [5] C. H. Bishop, J. S. Whitaker and L. Lei, Gain form of the Ensemble Transform Kalman Filter and its relevance to satellite data assimilation with model space ensemble covariance localization, *Mon. Wea. Rev.*, **145** (2017), 4575–4592.
- [6] C. M. Bishop, Training with noise is equivalent to Tikhonov regularization, *Neural Computation*, **7** (1995), 108–116.

- [7] M. Bocquet, Localization and the iterative ensemble Kalman smoother, *Q. J. R. Meteorol. Soc.*, **142** (2016), 1075–1089.
- [8] M. Bocquet, J. Brajard, A. Carrassi and L. Bertino, Data assimilation as a learning tool to infer ordinary differential equation representations of dynamical models, *Nonlin. Processes Geophys.*, **26** (2019), 143–162.
- [9] M. Bocquet, J. Brajard, A. Carrassi and L. Bertino, Bayesian inference of chaotic dynamics by merging data assimilation, machine learning and expectation-maximization, *Foundations of Data Science*, **2** (2020), 55–80.
- [10] M. Bocquet and A. Carrassi, Four-dimensional ensemble variational data assimilation and the unstable subspace, *Tellus A*, **69** (2017), 1304504.
- [11] M. Bocquet and A. Farchi, On the consistency of the perturbation update of local ensemble square root Kalman filters, *Tellus A*, **71** (2019), 1–21.
- [12] M. Bocquet, K. S. Gurumoorthy, A. Apte, A. Carrassi, C. Grudzien and C. K. R. T. Jones, Degenerate Kalman filter error covariances and their convergence onto the unstable subspace, *SIAM/ASA J. Uncertainty Quantification*, **5** (2017), 304–333.
- [13] M. Bocquet and P. Sakov, Combining inflation-free and iterative ensemble Kalman filters for strongly nonlinear systems, *Nonlin. Processes Geophys.*, **19** (2012), 383–399.
- [14] M. Bocquet and P. Sakov, Joint state and parameter estimation with an iterative ensemble Kalman smoother, *Nonlin. Processes Geophys.*, **20** (2013), 803–818.
- [15] J. Brajard, A. Carrassi, M. Bocquet and L. Bertino, Combining data assimilation and machine learning to emulate a dynamical model from sparse and noisy observations: a case study with the Lorenz 96 model, *J. Comput. Sci.*, URL <http://arxiv.org/pdf/2001.01520.pdf>, Accepted for publication.
- [16] S. L. Brunton, J. L. Proctor and J. N. Kutz, Discovering governing equations from data by sparse identification of nonlinear dynamical systems, *PNAS*, **113** (2016), 3932–3937.
- [17] M. Carlu, F. Ginelli, V. Lucarini and A. Politi, Lyapunov analysis of multiscale dynamics: the slow bundle of the two-scale Lorenz 96 model, *Nonlin. Processes Geophys.*, **26** (2019), 73–89.
- [18] A. Carrassi, M. Bocquet, L. Bertino and G. Evensen, Data assimilation in the geosciences: An overview on methods, issues, and perspectives, *WIREs Climate Change*, **9** (2018), e535.
- [19] C. L. Defforge, B. Carissimo, M. Bocquet, R. Bresson and P. Armand, Improving CFD atmospheric simulations at local scale for wind resource assessment using the iterative ensemble Kalman smoother, *J. Wind. Eng. Ind. Aerod.*, **189** (2019), 243–257.
- [20] P. D. Dueben and P. Bauer, Challenges and design choices for global weather and climate models based on machine learning, *Geosci. Model Dev.*, **11** (2018), 3999–4009.
- [21] G. Evensen, *Data Assimilation: The Ensemble Kalman Filter*, 2nd edition, Springer-Verlag Berlin Heidelberg, 2009.
- [22] R. Fablet, S. Ouala and C. Herzet, Bilinear residual neural network for the identification and forecasting of dynamical systems, in *EUSIPCO 2018, European Signal Processing Conference*, Rome, Italy, 2018, 1–5.
- [23] A. Farchi and M. Bocquet, On the efficiency of covariance localisation of the ensemble Kalman filter using augmented ensembles, *Front. Appl. Math. Stat.*, **5** (2019), 3.
- [24] E. Fertig, B. S.-J., H. B., O. E., S. I., J. Aravéquia, K. E., H. Li and J. Liu, Observation bias correction with an ensemble Kalman filter, *Tellus A*, **61** (2009), 210–226.
- [25] A. Fillion, M. Bocquet, S. Gratton, S. Gürol and P. Sakov, An iterative ensemble Kalman smoother in presence of additive model error, *SIAM/ASA J. Uncertainty Quantification*, **8** (2020), 198–228.
- [26] G. Gaspari and S. E. Cohn, Construction of correlation functions in two and three dimensions, *Q. J. R. Meteorol. Soc.*, **125** (1999), 723–757.
- [27] C. Grudzien, A. Carrassi and M. Bocquet, Chaotic dynamics and the role of covariance inflation for reduced rank Kalman filters with model error, *Nonlin. Processes Geophys.*, **25** (2018), 633–648.
- [28] T. M. Hamill, J. S. Whitaker and C. Snyder, Distance-dependent filtering of background error covariance estimates in an ensemble Kalman filter, *Mon. Wea. Rev.*, **129** (2001), 2776–2790.
- [29] R. A. Horn and C. R. Johnson, *Matrix analysis*, 2nd edition, Cambridge university press, 2013.
- [30] P. L. Houtekamer and H. L. Mitchell, A sequential ensemble Kalman filter for atmospheric data assimilation, *Mon. Wea. Rev.*, **129** (2001), 123–137.

- [31] W. W. Hsieh and B. Tang, Applying neural network models to prediction and data analysis in meteorology and oceanography, *Bull. Amer. Meteor. Soc.*, **79** (1998), 1855–1870.
- [32] X.-M. Hu, F. Zhang and J. W. Nielsen-Gammon, Ensemble-based simultaneous state and parameter estimation for treatment of mesoscale model error: A real-data study, *Geophys. Res. Lett.*, **37** (2010), L08802.
- [33] B. R. Hunt, E. J. Kostelich and I. Szunyogh, Efficient data assimilation for spatiotemporal chaos: A local ensemble transform Kalman filter, *Physica D*, **230** (2007), 112–126.
- [34] A. H. Jazwinski, *Stochastic Processes and Filtering Theory*, Academic Press, New-York, 1970.
- [35] N. B. Kovachki and A. M. Stuart, Ensemble Kalman inversion: a derivative-free technique for machine learning tasks, *Inverse Problems*, **35** (2019), 095005.
- [36] H. Koyama and M. Watanabe, Reducing forecast errors due to model imperfections using ensemble Kalman filtering, *Mon. Wea. Rev.*, **138** (2010), 3316–3332.
- [37] R. Lguensat, P. Tandeo, P. Ailliot, M. Pulido and R. Fablet, The analog data assimilation, *Mon. Wea. Rev.*, **145** (2017), 4093–4107.
- [38] Z. Long, Y. Lu, X. Ma and B. Dong, PDE-Net: learning PDEs from data, in *Proceedings of the 35th International Conference on Machine Learning*, 2018.
- [39] E. N. Lorenz, Designing chaotic models, *J. Atmos. Sci.*, **62** (2005), 1574–1587.
- [40] E. N. Lorenz and K. A. Emanuel, Optimal sites for supplementary weather observations: simulation with a small model, *J. Atmos. Sci.*, **55** (1998), 399–414.
- [41] E. Ott, B. R. Hunt, I. Szunyogh, A. V. Zimin, E. J. Kostelich, M. Corazza, E. Kalnay, D. J. Patil and A. Yorke, A local ensemble Kalman filter for atmospheric data assimilation, *Tellus A*, **56** (2004), 415–428.
- [42] J. Paduart, L. Lauwers, J. Swevers, K. Smolders, J. Schoukens and R. Pintelon, Identification of nonlinear systems using polynomial nonlinear state space models, *Automatica*, **46** (2010), 647–656.
- [43] J. Pathak, B. Hunt, M. Girvan, Z. Lu and E. Ott, Model-free prediction of large spatiotemporally chaotic systems from data: A reservoir computing approach, *Phys. Rev. Lett.*, **120** (2018), 024102.
- [44] P. N. Raanes, A. Carrassi and L. Bertino, Extending the square root method to account for additive forecast noise in ensemble methods, *Mon. Wea. Rev.*, **143** (2015), 3857–38730.
- [45] S. Rasp, Coupled online learning as a way to tackle instabilities and biases in neural network parameterizations: general algorithms and Lorenz96 case study (v1.0), *Geosci. Model Dev.*, **13** (2020), 2185–2196.
- [46] Y. M. Ruckstuhl and T. Janjić, Parameter and state estimation with ensemble Kalman filter based algorithms for convective-scale applications, *Q. J. R. Meteorol. Soc.*, **144** (2018), 826–841.
- [47] J. J. Ruiz, M. Pulido and T. Miyoshi, Estimating model parameters with ensemble-based data assimilation: A review, *J. Meteorol. Soc. Japan*, **91** (2013), 79–99.
- [48] P. Sakov and L. Bertino, Relation between two common localisation methods for the EnKF, *Comput. Geosci.*, **15** (2011), 225–237.
- [49] P. Sakov, J.-M. Haussaire and M. Bocquet, An iterative ensemble Kalman filter in presence of additive model error, *Q. J. R. Meteorol. Soc.*, **144** (2018), 1297–1309.
- [50] P. Sakov, D. S. Oliver and L. Bertino, An iterative EnKF for strongly nonlinear systems, *Mon. Wea. Rev.*, **140** (2012), 1988–2004.
- [51] S. Scher and G. Messori, Generalization properties of feed-forward neural networks trained on Lorenz systems, *Nonlin. Processes Geophys.*, **26** (2019), 381–399.
- [52] J. A. Weyn, D. R. Durran and R. Caruana, Using deep learning to predict gridded 500-hPa geopotential height from historical weather data, *Journal of Advances in Modeling Earth Systems*, **11** (2019), 2680–2693.
- [53] J. S. Whitaker and T. M. Hamill, Ensemble data assimilation without perturbed observations, *Mon. Wea. Rev.*, **130** (2002), 1913–1924.

E-mail address: marc.bocquet@enpc.fr

E-mail address: alban.farchi@enpc.fr

E-mail address: quentin.malartic@enpc.fr